

# Adiabatic nucleus-nucleus potential at near-barrier energies from selfconsistent calculations

Janusz Skalski

*A. Soltan Institute for Nuclear Studies,  
ul. Hoża 69, PL- 00 681, Warsaw, Poland* \*

(Dated: November 19, 2018)

Adiabatic fusion potentials, extended well into compound nucleus region, are calculated for a number of reactions within the static Hartree-Fock method with the Skyrme SkM\* interaction. The calculated fusion barriers agree quite well with the data, in spite of considerable errors in reaction  $Q$  values. This suggests some error cancellation, possibly with the relative kinetic energy term. Calculated barrier heights are consistent with the idea of fusion hindrance in tip collisions. Adiabatic potentials differ considerably from the results of the frozen density approximation. We briefly discuss relative positions and heights of the fusion and fission potentials and speculate on their possible connection with the fusion hindrance for large  $Z_T Z_P$ .

PACS numbers: 25.70.Jj,21.60.Jz

## I. INTRODUCTION

Entrance channel potential is one of the principal ingredients in the description of heavy ion collisions. It controls not only the capture probability, but is also related to a substantial hindrance of the compound nucleus (CN) formation, observed experimentally as a large probability of quasifission in reactions between targets and projectiles with  $Z_T Z_P > 1800$ . In this way it is crucial for prospects of the synthesis of the heaviest elements.

Up to now, calculations of the entrance channel potentials were performed mostly within some phenomenological models. The mean field Hartree-Fock (HF) methods were applied only with the assumption of frozen densities (see [1, 2] for recent examples), which involves approximations spoiling selfconsistency. The same assumption underlies the nuclear matter approach, see e.g. [3]. It was sometimes argued that such instantaneous, diabatic fusion barrier should be expected in actual heavy ion collisions due to the short time scale involved in passing over the barrier. Nevertheless, too high barriers and unrealistic, strongly repulsive potentials obtained in the frozen density regime [1, 2] point to a limited relevance of this method. We think that the adiabatic potential is a necessary ingredient in the selfconsistent study of nuclear fusion in much the same way as the static barrier is a necessary first step in a study of nuclear fission.

In this work, we have performed HF calculations for a number of target-projectile combinations and found the adiabatic nucleus-nucleus potential and (outer) fusion barrier. As might be expected, the adjustment of the nuclear matter to the mutual interaction of target and projectile gives markedly different results from those of the frozen density approach.

Within the mean field, for a deformed target or projectile, there are many fusion barriers, depending on the relative orientation of fragments. We have calculated potentials for tip and side collisions, i.e. for the configuration with the symmetry axis of the deformed fragment parallel and perpendicular to the relative distance vector. Effects of the fragment orientation and deformation on fusion were proposed in [4]. Quite recently, experimental evidence was presented [5, 6, 7] showing that at least part of the CN formation hindrance is related to the dominance of quasifission in tip collisions.

We have used mostly the Skyrme SkM\* interaction [8], originally invented to properly fit the fission barriers. We are aware of previous HF calculations of the potential energy in a dinuclear regime, like e.g. [9] (see also recent work [10]), however, their objective was nuclear scission, where deformations of separating fragments much differ from those expected in the fusion entrance channel.

The aim of this paper is twofold. First, we provide some systematics of the selfconsistent fusion barriers and check against the experimental data and the recent calculations within the frozen density regime [1] with the same interaction. In our study, we include some systems with well measured fusion cross sections as well as reactions on  $^{208}\text{Pb}$  target of the type studied in GSI Darmstadt [11, 12] and  $^{48}\text{Ca}$ -induced reactions used in recent experiments at JINR in Dubna [13, 14, 15], both reported as leading to the synthesis of the heaviest elements. Second, we look

---

\*Electronic address: jskalski@fuw.edu.pl

for a relative position (deformations) and height of the fusion channels with respect to the fission valley to figure out quantum transitions implied by the fusion process. Our original motive was to find whether the adiabatic energy surface offers some clue to the fusion hindrance.

Some preliminary results of this study have been published in [16]. Differences between the present barriers and those in [16] come from more extensive HF iterations and the improved numeric treatment of kinetic energy.

## II. METHOD OF CALCULATIONS

We calculate static potentials, which means that we neglect currents and other time-odd quantities in the Skyrme energy functional and consider time-reversal invariant HF states. This seems reasonable at energies close to the Coulomb barrier. The potential between nuclei 1 and 2 in the central collision is then

$$V(R) = E(R) + B_1 + B_2, \quad (1)$$

where  $E(R)$  is the (negative) HF energy of a dinuclear complex at the distance  $R$  and  $B_i$  are the (positive) binding energies of target and projectile. In order to have a numerically consistent treatment,  $B_i$ ,  $i = 1, 2$ , and  $E(R)$  are calculated with the same HF code. In the present calculation pairing is neglected.

The HF equations have been solved on a spatial mesh of a size proper to the colliding system. Our code assumes two plane symmetries, i.e. it allows for the mass asymmetry along one direction. We consider tip and side collisions, with the angle between the symmetry axis of a deformed nucleus and the line connecting centers of two fragments equal to  $0^\circ$  and  $90^\circ$ .

Initially, two sets of wave functions corresponding to two fragments are placed at a chosen distance being an integer multiple of the mesh spacing (0.69 or 0.77 fm). The HF equations are solved by the imaginary-time evolution. Wave functions are kept orthonormal and this enforces the Pauli principle. For fragments placed close enough, the necessary rearrangement of orbitals occurs already at the beginning of the HF procedure and avoids higher than normal densities. Final wave functions correspond to the local minima of the energy functional to which the initial configuration converged. For compact configurations of the CN, i.e. small  $R$ , there may be quite a few such minima, corresponding to different valleys in the nuclear energy (hyper-)surface. Thus, in contrast to the fusion barrier, the entrance channel (fusion) potential  $V(R)$  is not unique. The distance  $R$  between two fragments is calculated as the distance between the mass centers of two half-spaces containing  $A_1$  and  $A_2$  nucleons.

Since HF states are superpositions of various total momentum eigenstates, one has to include the center of mass (cm) kinetic energy correction. The expectation value of the cm kinetic energy for an  $N$ -fermion Slater determinant reads

$$E_{cm}(N) = \frac{1}{2MN} \left( \sum_{k=1}^N \langle k | \mathbf{p}^2 | k \rangle - \sum_{k \neq l}^N | \langle k | \mathbf{p} | l \rangle |^2 \right), \quad (2)$$

with  $k, l$  labelling occupied single particle states. Only exchange two-body terms are present in Eq.(2) as the diagonal matrix elements of momentum vanish in the time-reversal invariant states. In most of the HF calculations two-body terms in  $E_{cm}$  are neglected (for a competent review of the cm corrections in HF see [17]). With the Skyrme SkM\* force,  $E_{cm}$  is taken as the average kinetic energy,  $\langle t \rangle = \sum_{k-occ} \langle k | \hat{t} | k \rangle / A$ .

Independently of the approximations made, for a Slater determinant describing two separated fragments with  $N_1$  and  $N_2$  nucleon wave functions,  $N_1 + N_2 = N$ , with vanishing mutual momentum overlaps,  $\langle k_1 | \mathbf{p} | k_2 \rangle = 0$ , one obtains the relation

$$E_{cm}(N_1) + E_{cm}(N_2) = E_{cm}(N) + \frac{N_2 E_{cm}(N_1) + N_1 E_{cm}(N_2)}{N}. \quad (3)$$

This implies that in any HF calculation which includes  $E_{cm}$ , the nucleus- nucleus potential  $V(R)$  of Eq.(1) will tend to the value of the second term on the right hand side of Eq.(3), when  $R$  tends to infinity. This term is just the expectation value of the kinetic energy of the relative motion of the two fragments. In order to preserve the usual meaning of the Coulomb barrier one has to subtract this asymptotic term in Eq.(1). Specifically, with the SkM\* force and for fragments with  $A_1$  and  $A_2$  nucleons,  $A_1 + A_2 = A$ , one has to subtract  $(A_2 \langle t_1 \rangle + A_1 \langle t_2 \rangle) / A$ .

This subtraction has been included in the frozen density calculations [1, 2]. However, it is surely incorrect when two fragments become one, i.e., for compact configurations of the system. As we do not know how kinetic energy of the relative motion of the fragments transforms into potential energy of the combined system, and still want to compare with the existing frozen density results, we also calculate  $V(R)$  normalized to zero at infinity. One has to keep in mind that such potential underestimates the true  $V(R)$ : the smaller the distance  $R$ , the larger the offset which

reaches  $-14$  to  $-18$  MeV at the CN ground state. The product  $Z_T Z_P$  controls the overlap of target and projectile at the fusion barrier: the larger  $Z_T Z_P$ , the larger the overlap. Hence, one can expect that  $E_{cm}$  correction, valid for separated fragments, produces too low fusion barriers for fragments with large  $Z_T Z_P$ .

### III. RESULTS AND DISCUSSION

Examples of entrance channel potentials are shown in Figs. 1,2. In Fig. 1 we show the tip- and side collision barrier for the  $^{244}\text{Pu} + ^{48}\text{Ca}$  reaction. Two results are shown, differing by the number of performed HF iterations. Adiabatic (lower) barriers were obtained after three long series of iterations, required in view of an inefficient convergence of the pure HF without pairing. Only one series of iterations produced the other (higher) plotted barriers. The quantities obtained in this way were in fact published in [16]. It is seen that an incomplete convergence in the true HF mimics to some extent the frozen density results [1, 3]: for systems with large  $Z_T Z_P$  there is a potential pocket inside the fusion barrier and  $V(R)$  rises steeply with decreasing  $R$ . In the frozen density method this results from a higher than normal density in the overlap region. In the HF, it is the initial orthogonalization which disturbs density in the overlap region and rises energy. A subsequent quenching is necessary to lose this excitation.

In quantitative terms, even non-fully adiabatic selfconsistent potentials are lower and rise much less steeply with decreasing  $R$  than the frozen density results. This rise vanishes in fully adiabatic potentials, as seen in Figs. 1,2. These potentials decrease with decreasing  $R$ , except for the superheavy systems, where the Coulomb barrier becomes a local plateau at the level of, or even below, the ground state of CN. In addition to the  $^{208}\text{Pb} + ^{70}\text{Zn}$  reaction, potentials with a plateau in the place of the barrier are obtained also for the  $^{208}\text{Pb} + ^{82}\text{Ge}$  and  $^{132}\text{Sn} + ^{132}\text{Sn}$  systems. A comparison of fusion barrier heights shows that for reactions on  $^{208}\text{Pb}$  and actinide targets leading to very heavy nuclei the adiabatic barriers are by 10-20 MeV lower than the frozen density ones [1] (see also Table 1). Taken at the face value, the adiabatic results suggest that, after passing the fusion barrier, systems with sufficiently low  $Z_P Z_T$  experience a steady driving force towards CN formation, while with increasing  $Z_T Z_P$  this force weakens and even changes to repulsion.

It may be noticed in Fig. 1 for the reaction  $^{244}\text{Pu} + ^{48}\text{Ca}$  that the shorter and higher side collision potential offers larger driving force towards CN than the longer but lower tip collision one. The difference in the barrier position for tip- and side collision for  $^{244}\text{Pu} + ^{48}\text{Ca}$  system,  $R_{tip} - R_{side}$ , is about 2 fm. Similar situation occurs for the reaction  $^{110}\text{Pd} + ^{110}\text{Pd}$  (Fig. 2), for which the tip-tip collision potential shows a plateau with fluctuations. On the other hand, the higher side-side collision barrier gives chance to a quite steep (20 MeV) slide towards CN pocket (see below). The potential for the  $^{208}\text{Pb} + ^{70}\text{Zn}$  reaction, on the other hand, does not provide any force in the CN direction. This could suggest that the entrance channel potentials give a better chance of fusion in the side collisions with prolate deformed actinide targets as compared to reactions on  $^{208}\text{Pb}$  target.

When comparing various results for barriers one has to remember that with rising  $Z_T Z_P$  1) the frozen density approach becomes poorer, 2) the correction for cm energy becomes questionable and may produce too low barriers, 3) the adiabaticity effect on the lowering of the barrier increases.

Calculated fusion barriers  $B_{cal}$ , taken as the locally highest value of  $V(R)$ , rounded to 0.5 MeV, are compared in Table 1 to the Bass interaction barriers [18] and to the recently given threshold barriers  $B_{thre}$  [19]. The interaction barriers are chosen here instead of the fusion barriers [18] since they much better approximate the experimental barriers for heavy systems. The threshold barriers [19] are derived from sufficiently detailed fusion data and should correspond to the calculated adiabatic barriers. The values of  $B_{thre}$  for the heaviest systems are based on the capture data [20]. For deformed targets, both the calculated tip and side (in parentheses) collision barriers are given. In order to appreciate excitation of a compound system at the fusion barrier we also give in Table 1 the experimental (or extrapolated) reaction  $Q$  values.

Out of nine threshold barriers, two are overestimated and six underestimated in the calculations by up to 4 MeV (it seems that  $B_{thre}$  for the  $^{238}\text{U} + ^{16}\text{O}$  reaction corresponds to tip collision [5]). One, for the  $^{238}\text{U} + ^{48}\text{Ca}$  reaction, is 6 MeV below the calculated side collision barrier and 11 MeV above the tip collision one. Although for two reactions leading to  $^{214}\text{Th}$  CN the barriers  $B_{thre}$  are not known exactly, their rough estimate from data [6] is possible. For the reaction  $^{182}\text{W} + ^{32}\text{S}$  the estimate agrees well with our  $B_{cal}$ , while for  $^{154}\text{Sm} + ^{60}\text{Ni}$  it seems close to the calculated tip collision barrier, although the lack of the low energy data causes large uncertainty. It should be stressed that the lack of observed evaporation residues (ERs) at  $E_{cm}=175$  and 182 MeV in the experiment [6] served as an argument for the fusion hindrance in tip collisions.

The fusion barrier calculated for the recently measured reaction  $^{132}\text{Sn} + ^{64}\text{Ni}$  is higher than  $B_{thre}$  suggested by the data [25], but lower than the Bass interaction barrier assumed in the coupled channels analysis there. The  $^{110}\text{Pd}$  nucleus, previously considered vibrational (see e.g. [22]), is now well established by the Coulomb excitation studies [26] as a rotor with deformation  $\beta_2 \approx 0.25$ . We have obtained a shallow prolate-deformed HF minimum at  $Q = 7.4$  b, consistent with this, and used it to calculate tip-tip and side-side collision barriers given in Fig. 2 and Table 1. The  $^{110}\text{Pd} + ^{110}\text{Pd} \rightarrow ^{220}\text{U}$  reaction is a very well known case of the severe fusion hindrance [27], at least by four orders of

magnitude. The lowest measured point at  $E_{cm} = 228$  MeV is already above the calculated side collision barrier.

For most reactions leading to superheavy nuclei there are too few data to extract threshold barriers, even from capture data. However, the data on evaporation residue formation give some upper bound on the height of the fusion barrier, as their production at  $E_{cm}$  below the lowest barrier is improbable. For  $^{208}\text{Pb}$  target, the  $^{271}110$  ERs were detected following reaction with  $^{64}\text{Ni}$  at  $E_{cm} = 235.3 - 238.2$  MeV [11, 28], while in reaction with  $^{70}\text{Zn}$  two observed  $^{277}112$  ERs were produced at  $E_{cm} = 257.2$  and 259.1 MeV [12]. In reactions with  $^{48}\text{Ca}$  projectiles on actinide targets, two ERs were observed in the reaction on  $^{238}\text{U}$  at  $E_{cm} = 190.5 - 193.9$  MeV [29], three events in the reaction on  $^{244}\text{Pu}$  target at  $E_{cm} = 194.5 - 202$  MeV [14, 30] and one event for  $^{248}\text{Cm}$  target at  $E_{cm} = 199.7 - 205.1$  MeV [15]. All these bombardment energies in the c.m. system are higher than our calculated barriers: by at least 6 and 13 MeV for  $^{64}\text{Ni}$  and  $^{70}\text{Zn}$  projectiles on  $^{208}\text{Pb}$  target, and by 2-3 MeV higher than the calculated side collision barriers for actinide targets.

Overall reasonable agreement of the calculated fusion barriers with data is quite astonishing in view of the deficiency shown by the SkM\* force in reproducing the experimental binding energies. As follows from our calculations and the recently calculated mass table [31] there is a large underestimation of binding for heavy and superheavy nuclei with the SkM\* force, e.g. about 9 MeV for  $^{182}\text{W}$  and  $^{244}\text{Pu}$ , but already about 14 MeV for  $^{256}\text{No}$ , and expected 18 MeV for  $^{292}114$ , according to usually fair estimates of the phenomenological Thomas-Fermi model [24]. Moreover, there are some errors specific to SkM\* force, like too large bindings of  $^{48}\text{Ca}$  (by 4 MeV) and  $^{132}\text{Sn}$  (by 7.5 MeV).

It is reasonable to ask about a correlation between errors in fusion barriers and those in reaction  $Q$  values. It turns out that the  $Q$  values are overestimated by up to 5 MeV for lighter compound systems, i.e. similar in magnitude but mostly opposite to the errors in barriers. However, for heavier compound systems the errors in barriers are much smaller than those in  $Q$  values, e.g.  $Q$  values are too large by about 11 MeV for  $^{90}\text{Zr} + ^{90}\text{Zr}$ , about 17 MeV for  $^{48}\text{Ca} + ^{208}\text{Pb}$ , expected about 13 MeV too large for  $^{48}\text{Ca} + ^{244}\text{Pu}$ . All this points to some error cancellation, which, as discussed in the previous section, might be related to the overestimated relative kinetic energy correction.

An intriguing question is whether the calculated potentials  $V(R)$  may be related quantitatively to the fusion hindrance seen in experiment. In [1], a sufficiently deep pocket in the frozen density potential  $V(R)$  was proposed as a necessary precondition for fusion. The quantification of this assertion is difficult, as the depth and the very existence of the pocket relies on the unrealistic frozen density intrinsic barrier, which exists e.g. already for  $^{90}\text{Zr} + ^{90}\text{Zr}$  and  $^{208}\text{Pb} + ^{48}\text{Ca}$  reactions, for which no fusion hindrance is experimentally observed [20, 21].

Reasoning intuitively, a relative situation and heights of fusion and fission valleys should be relevant for prospects of fusion: to be captured in the CN configuration, a system must pass inside the CN fission barrier. In order to gain some orientation in this respect, a more detailed calculations have been performed for a few nuclei. The results for  $^{292}114$  ( $^{244}\text{Pu} + ^{48}\text{Ca}$  reaction) are shown in Fig. 3. When showing fission and fusion barriers in one figure the kinetic energy of the fragment relative motion *has not been subtracted* from the fusion barrier. Instead of the distance  $R$  between two fragments the quadrupole moment  $Q_{20}$  of the compound system is shown on the abscissa. The calculated mass- and axially symmetric fission barrier of 15 MeV is heavily overestimated as compared to the experimental estimate  $B_{fis} \approx 6.5$  MeV [32], consistent with the Strutinsky method calculations [33]. This comes partly from the lack of pairing and neglect of nonaxiality. Accounting for both these effects still leaves a few MeV discrepancy between the data and the barrier obtained with the SkM\* force. Similarly, the second hump of the barrier will be lowered by pairing and mass-asymmetry. Therefore, Fig. 3 gives a general idea about relative position of important points of the nuclear energy landscape rather than exact barrier heights.

The tip-collision potential lies below the second hump of the fission barrier and corresponds to a sizable mass asymmetry, increasing with  $Q_{20}$ . In the right portion of the figure, we extend fission barrier to mass asymmetry by showing cuts through the potential energy surface at fixed  $Q_{20} = 100, 125$  and  $140$  b vs. octupole moment  $Q_{30}$ . It is seen that the mass-asymmetric minimum becomes energetically well separated from the symmetric fission valley with increasing  $Q_{20}$ . The nuclear states building fusion potential are very close to the states in the fission valley with alike quadrupole and octupole moments, e.g. at  $Q_{20} = 140$  b and  $Q_{30} \approx 25 \cdot 10^3$  fm $^3$ , at  $Q_{20} \approx 125$  b and  $Q_{30} \approx 20 \cdot 10^3$  fm $^3$  and at  $Q_{20} \approx 100$  b and  $Q_{30} \approx 12 \cdot 10^3$  fm $^3$ . Slight differences in energy (1-2 MeV) come from differences in necking. One can say that the tip collision potential arises from traversing potential energy surface, in this case not quite along the conditional minima at fixed  $Q_{20}$ , as these lie slightly lower.

This overall picture suggests that, after surpassing the fusion barrier, the system has a good chance to fall inside the outer fission barrier. If some energy is lost to excitation on the way, it may be stopped at the higher inner barrier. One may expect that fusion in the tip collisions is hindered in this case.

The side collision potential lies above both humps of the fission barrier and, after surpassing the fusion barrier, the system can roll down all the way to the CN ground state, even if some energy is transferred to excitation. (Looking at Fig. 3 it is good to remember that the side collision barrier has a large axial asymmetry.)

For  $^{256}\text{No}$  ( $^{208}\text{Pb} + ^{48}\text{Ca}$  reaction, not shown) the mass-asymmetric entrance channel potential leads inside the higher, inner hump of the mass-symmetric fission barrier. The calculated height of the latter, 15 MeV, again exceeds the experimental estimate consistent with the value  $\approx 8$  MeV obtained in the Strutinsky-like studies, but is similar to

the barrier (12.6 MeV) calculated for  $^{254}\text{No}$  with SkLy4 force [34]. The lower, secondary hump of the fission barrier does not play any role. Therefore, one should not expect drastic fusion hindrance in this reaction.

The above are examples of possible qualitative inferences one can make from knowing adiabatic energy surfaces. Surely, the concept that the relative situation of the fusion potential and fission barriers has relation to fusion hindrance requires further study. It is plausible that not only nuclear configurations, but also configuration changes which occur with some probability, are involved in the resulting loss of the probability of fusion.

Conclusions of this work may be stated as follows:

- Adiabatic fusion barriers calculated with SkM\* force compare rather well with experiment, anyway much better than the frozen density results.
- The barriers compare with experiment much better than the reaction  $Q$  values for heavy and superheavy systems. This may suggest that there is some error cancellation: subtraction of a too large relative kinetic energy makes up for too large reaction  $Q$  values.
- The rise of the potential  $V(R)$  with decreasing  $R$  seen in the frozen density or not fully adiabatic calculations vanishes in adiabatic potentials, except for the heaviest CN where the fusion barrier top lies below the ground state. Thus, the relation of this rise to the fusion hindrance is not clear.
- The comparison of our calculated barrier heights to data supports the idea that in reactions with large  $Z_T Z_P$  and deformed fragments fusion is suppressed in tip collisions in spite of the substantially lower fusion barrier.
- Judging from forces driving towards the CN minimum, the formation of superheavy CN may be easier in side collisions with deformed actinides used in JIHR Dubna, than in reactions with spherical targets used in GSI Darmstadt (without considering survival probability).

The latter two points suggest that the size of a necessary rearrangement of the nuclear matter drop is more vital for fusion than the barrier heights. One may wonder whether some measure of this rearrangement is not a proper variable to describe the fusion hindrance. One such variable could be  $R_{fus} - R_{fis}$ , where the position of the inner fission barrier is relevant. Obviously, these speculations call for a more detailed study, including multidimensional energy surfaces and pairing.

---

- [1] V.Yu Denisov and W. Nörenberg, Eur. Phys. Journal A 15 (2002) 375
- [2] A. Dobrowolski, K. Pomorski and J. Bartel, Nucl. Phys. A 729 (2003) 713, nucl-th/0303074
- [3] J. Dąbrowski, H. S. Köhler and J. Roźnek, Acta Phys. Pol. B 34 (2003) 4257
- [4] A. Iwamoto, P. Möller, J. Rayford Nix and H. Sagawa, Nucl. Phys A 596 (1996) 329
- [5] D.J. Hinde et al., Phys. Rev. Lett. 74 (1995) 1295
- [6] S. Mitsuoka et al., Phys. Rev. C 62 (2000) 054603
- [7] K. Nishio et al., Phys. Rev. C 62 (2000) 014602
- [8] J. Bartel et al., Nucl. Phys. A 386 (1982) 79
- [9] J. F. Berger, M. Girod and D. Gogny, Nucl. Phys. A 502 (1989) 85c
- [10] M. Warda, J.L. Egido, L.M. Robledo and K. Pomorski, Phys. Rev. C66 (2002) 014310
- [11] S. Hoffman, Rep. Prog. Phys. 61 (1998) 639
- [12] S. Hoffmann and G. Münzenberg, Rev. Mod. Phys. 72 (2000) 733
- [13] Yu. Ts. Oganessian et al., Nature (London) 400 (1999) 242
- [14] Yu. Ts. Oganessian et al., Phys. Rev. Lett. 83 (1999) 3154
- [15] Yu. Ts. Oganessian et al., Phys. Rev. C 63 (2001) 011301(R)
- [16] J. Skalski, Acta Phys. Pol. B 34 (2003) 1977
- [17] M. Bender, K. Rutz, P.-G. Reinhard and J. A. Maruhn, Eur. Phys. J. A 7 (2000) 467
- [18] R. Bass, Nucl. Phys. A 231 (1974) 45
- [19] K. Siwek-Wilczyńska and J. Wilczyński, Phys. Rev C 64 (2001) 024611
- [20] M.G. Itkis et al., in "Fusion Dynamics at the Extremes", ed. Yu. Ts. Oganessian and V.I. Zagrebaev, (World Scientific, 2001), p. 93
- [21] J.G. Keller et al., Nucl. Phys. A 452 (1986) 173
- [22] A. M. Stefanini et al., Phys. Rev. C 52 (1995) R1727
- [23] G. Audi and A.H. Wapstra, Nucl. Phys. A 595 (1995) 409
- [24] W.D. Myers and W.J. Swiatecki, Nucl. Phys. A 601 (1996) 141, report LBL-36803 (1994)
- [25] J. F. Liang et al., Phys. Rev. Lett. 91 (2003) 152701
- [26] D. Cline, Ann. Rev. Nucl. Part. Sci. 36 (1986) 683
- [27] W. Morawek et al., Z. Phys. A 341 (1991) 75
- [28] T. Ginter et al., Phys. Rev. C 67 (2003) 064609
- [29] Yu. Ts. Oganessian et al., in "Fusion Dynamics at the Extremes", ed. Yu. Ts. Oganessian and V.I. Zagrebaev, (World Scientific, 2001), p. 81

- [30] Yu. Ts. Oganessian et al., Phys. Rev. C 62, 041604(R) (2000), Yu. Ts. Oganessian et al., in "Fusion Dynamics at the Extremes", ed. Yu. Ts. Oganessian and V.I. Zagrebaev, (World Scientific, 2001), p. 65
- [31] M. V. Stoitsov, J. Dobaczewski, W. Nazarewicz, S. Pittel and D. J. Dean, Phys. Rev. C 68 (2003) 054312, nucl-th/0307049
- [32] M. G. Itkis, Yu. Ts. Oganessian and V. I. Zagrebaev, Phys. Rev. C 65 (2002) 044602
- [33] R. Smolaićzuk, Phys. Rev. C 56 (1997) 812
- [34] T. Duget, P. Bonche and P-H. Heenen, Nucl. Phys. A 679 (2001) 427

TABLE 1 - Calculated fusion barriers for tip (side) collisions in MeV vs. threshold [19] and Bass *interaction* (not fusion) barriers [18]. Threshold barrier for  $^{90}\text{Zr}+^{90}\text{Zr}$  is inferred from [21], that for  $^{238}\text{U}+^{16}\text{O}$  from [5], and for  $^{110}\text{Pd}+^{32}\text{S}$  from [22]. Reaction  $Q$  values (experimental/extrapolated [23], or predicted (with asterisk) [24]) are given in column 2.

System	$Q$	$B_{cal}$	$B_{thre}$	$B_{Bass}^{int}$
$^{40}\text{Ca}+^{40}\text{Ca}$	14.3	52	$50.2\pm 0.2$	52.5
$^{64}\text{Ni}+^{64}\text{Ni}$	48.8	86.5	$89.5\pm 0.3$	94.5
$^{90}\text{Zr}+^{40}\text{Ca}$	57.3	92	$92.7\pm 0.6$	97.7
$^{96}\text{Zr}+^{40}\text{Ca}$	41.1	85	$87.5\pm 0.3$	96.6
$^{90}\text{Zr}+^{90}\text{Zr}$	157.3	175	$\sim 175.85$	181.0
$^{110}\text{Pd}+^{32}\text{S}$	35.4	78(79.5)	$80.4\pm 0.2$	88.9
$^{110}\text{Pd}+^{110}\text{Pd}$	199.7	200(222.5)	-	228.3
$^{182}\text{W}+^{32}\text{S}$	84.9	121.5(124)	-	134.3
$^{154}\text{Sm}+^{60}\text{Ni}$	147.6	170(185.5)	-	191.5
$^{238}\text{U}+^{16}\text{O}$	38.3	67(71)	$\sim 71$	82.9
$^{132}\text{Sn}+^{64}\text{Ni}$	111.1	147	-	155.7
$^{132}\text{Sn}+^{132}\text{Sn}$	260.8 *	254.5	-	257.4
$^{208}\text{Pb}+^{48}\text{Ca}$	153.8	170.5	$169\pm 2$	176.1
$^{208}\text{Pb}+^{64}\text{Ni}$	225.1	229	-	241.3
$^{208}\text{Pb}+^{70}\text{Zn}$	244.9 *	244	-	256.3
$^{208}\text{Pb}+^{82}\text{Ge}$	262.5 *	260.5	-	268.8
$^{238}\text{U}+^{48}\text{Ca}$	160.8 *	171(188)	$182\pm 2$	193.8
$^{244}\text{Pu}+^{48}\text{Ca}$	163.0 *	174(192)	-	197.3
$^{248}\text{Cm}+^{48}\text{Ca}$	169.3 *	183(196.5)	-	201.0
$^{250}\text{Cf}+^{48}\text{Ca}$	177.0 *	187.5(201)	-	205.1

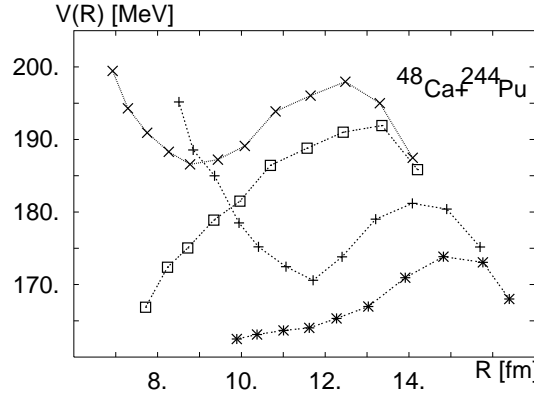


FIG. 1: Partially and fully adiabatic potentials for  $^{244}\text{Pu} + ^{48}\text{Ca}$  tip (pluses, stars) and side (crosses, squares) collision obtained with Skyrme SkM\* force.

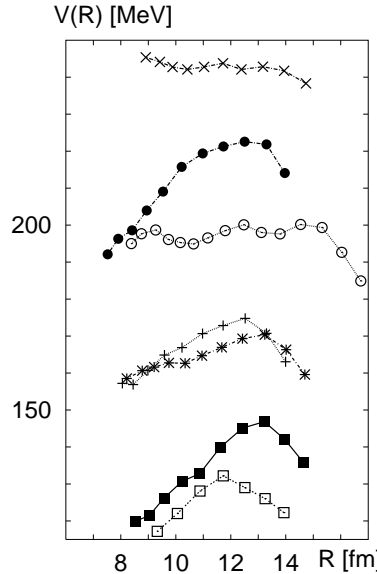


FIG. 2: Adiabatic nucleus-nucleus potentials for the reactions:  $^{90}\text{Zr} + ^{40}\text{Ca}$  (shifted up by 40 MeV, open squares),  $^{132}\text{Sn} + ^{64}\text{Ni}$  (full squares),  $^{208}\text{Pb} + ^{48}\text{Ca}$  (stars),  $^{90}\text{Zr} + ^{90}\text{Zr}$  (pluses),  $^{110}\text{Pd} + ^{110}\text{Pd}$  tip-tip (open circles) and side-side collision (full circles) and  $^{208}\text{Pb} + ^{70}\text{Zn}$  (crosses).

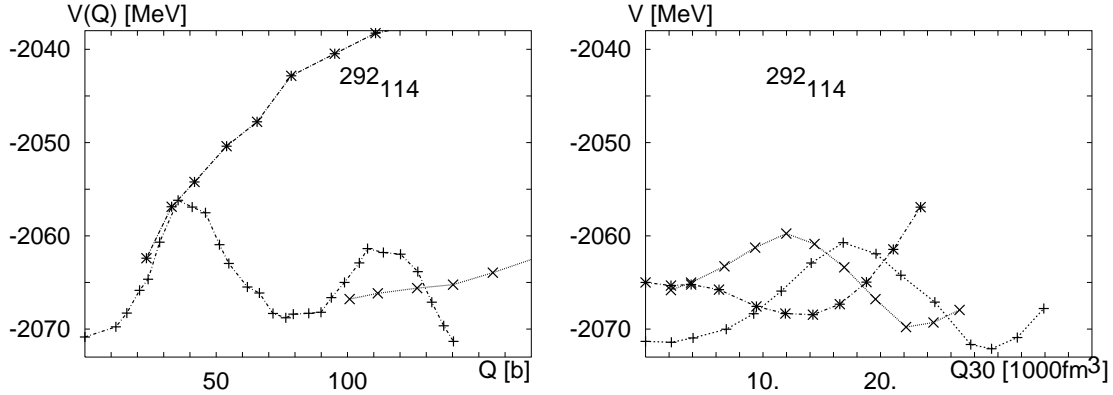


FIG. 3: Left panel: Mass-symmetric fission barrier (pluses) and fusion barriers for the  $^{48}\text{Ca}$ -induced reaction (tip collision - crosses, side collision - stars) for the compound system  $^{292}\text{114}$ . Right panel: fission valley in the same system vs. octupole moment  $Q_{30}$  for  $Q_{20} = 100$  b (stars), 125 b (crosses) and 140 b (pluses) .